Optics and Spectroscopy, Vol. 96, No. 3, 2004, pp. 328–334. Translated from Optika i Spektroskopiya, Vol. 96, No. 3, 2004, pp. 373–379.

ATOMIC SPECTROSCOPY

Zeeman Effect on the Hyperfine Structure of the D_1 Line of a Submicron Layer of ^{87}Rb Vapor

D. G. Sarkisyan*, A. V. Papoyan*, T. S. Varzhapetyan*, K. Blush, and M. Auzinsh****

** Institute for Physical Research, National Academy of Sciences of Armenia, Ashtarak-2, 378410 Armenia*

*** Department of Physics, Latvian University, Riga, LV-1586 Latvia*

Received May 20, 2003

Abstract—An extremely thin cell with a wedge gap was developed that makes it possible to form a column of Rb atom vapor with thickness in the range from 100 to 600 nm. It is experimentally shown that the use of this cell, along with commercially available diode lasers, allows one to spectrally resolve individual transitions between the Zeeman sublevels of the hyperfine structure of the ^{87}Rb D_1 line (transitions $F_g = 1, 2 \longrightarrow F_e = 1, 2$) in the resonance fluorescence spectrum in the presence of an external magnetic field ($B \approx 200$ G). This makes it possible to realize systems consisting of nondegenerate atomic levels. For comparison, it is shown that transitions between the Zeeman sublevels in the fluorescence spectrum obtained with the aid of a conventional cell (1–10 cm long) in an external magnetic field with $B \sim 200$ G remain completely masked by the Doppler-broadened profile. The results obtained can be used for the creation of a simple magnetometer based on an extremely thin cell with Rb vapor for the measurement of magnetic fields with a submicron local spatial resolution. © *2004 MAIK "Nauka/Interperiodica".*

1. INTRODUCTION

In recent years, a series of studies have been devoted to the spectroscopy of atomic vapors with the layer thickness $L \sim 10$–1000 μm [1–8]. It is noteworthy that, even at $L \sim 10$ μm, the sub-Doppler structure manifests itself under resonance pumping with a single laser beam [1]; however, for this structure to be revealed, the laser radiation must be additionally frequency-modulated [1–3].

Recently, it was shown that the use of an extremely thin cell (ETC) in which the thickness of the atomic vapor column is $L \sim 150$–300 nm and an ordinary laser diode (without frequency modulation) is sufficient for resolving the hyperfine atomic transitions of the D_2 line of Cs [9]. It is important that the resonance fluorescence and absorption have linear character (versus the pumping intensity) up to intensities of 100 mW/cm^2 [9] and, in contrast to the absorption saturation spectroscopy, based on a strongly nonlinear process, allow one to measure the probabilities of individual hyperfine atomic transitions.

As was noted in [9], the sub-Doppler width of atomic transitions in a ETC is narrower in the case of fluorescence than in the case of absorption, and, hence, in some cases, it is more reasonable to use the resonance fluorescence spectra.

The aim of the present paper is to study the possibility of complete spectral resolution of the transitions between Zeeman sublevels in the fluorescence spectrum using a ETC with Rb in comparatively weak magnetic fields. The conditions that are favorable for better spectral resolution of Zeeman components are as follows: the Landé g_F factors for the lower (ground) F_g and upper (excited) F_e hyperfine levels should have different signs and be as large as possible to increase the frequency shift; the dependence of the frequency shift on the magnetic field should be close to a linear dependence (so that the neighboring Zeeman levels do not overlap and are separated in frequency at all magnetic fields); the frequency spacing between the components of the hyperfine structure of both the lower and the upper levels should be as large as possible; and the values of F_g and F_e should be small, so that the number of magnetic sublevels will be small. From this point of view, the systems of the $F_g = 1, 2 \longrightarrow F_e = 1, 2$ transitions of the D_1 line of ^{87}Rb are the most convenient.

It should be noted that the analogous direct spectral resolution of Zeeman transitions in cells of ordinary (centimeter) lengths can be achieved only in strong magnetic fields, when the Zeeman shift exceeds the Doppler broadening of the spectral components. In [10], a magnetic field with a strength exceeding 1000 G was applied for the spectral resolution of Zeeman components in an ~1-cm cell with Rb vapor. In weaker magnetic fields, Zeeman components can be separated using indirect methods. For example, the authors of [11] used the selective reflection process for the spectral resolution of Zeeman transitions in Cs vapors (in a cell about 1 cm long) in a magnetic field.

0030-400X/04/9603-0328$26.00 © 2004 MAIK "Nauka/Interperiodica"

2. EXPERIMENTAL

2.1. The Design of the Extremely Thin Cell

As was shown in [7, 8], the best sub-Doppler spectral resolution is achieved at the cell thickness $L = \lambda/2$, where λ is the wavelength of the laser radiation. To satisfy this condition, we used a ETC with a wedge gap between the windows, so that the range of its thickness covered the desired value.

The ETC construction is similar to that described in [9], but has several distinctions. The windows, 30 mm in diameter and 3 mm thick, were made from $Y_3Al_5O_{12}$ garnet, which is chemically resistant to the vapors of alkali metals. To form the wedge gap, an Al_2O_3 strip ~600 nm thick, 10 mm long, and 1 mm wide (instead of the ring-shaped Al_2O_3 layer used in [9]) was deposited on the surface of one window in its lower part. Prior to the deposition, a hole 2 mm in diameter was drilled in the bottom of the windows, into which a tube of the same diameter and ~50 mm long, made of commercial sapphire, was inserted. Then, the entire construction was assembled and glued in a vacuum furnace [12]. After the gluing, a glass extension was sealed in the sapphire tube [13], and the ETC was filled with a natural mixture of ^{85}Rb and ^{87}Rb, as done for an ordinary glass cell. The amount of rubidium was chosen so that the sapphire tube, with an inner diameter of about 1 mm, was almost completely filled. After sealing off of the ETC, the glass tube was 5–6 mm long. As was shown in [14], the rubidium vapor pressure is determined by the temperature of the upper edge of the metal rubidium column in the sapphire tube. Varying the heater construction, one can achieve the following limiting thermal conditions: a temperature at the top upper edge of the metal Rb column of approximately 500°C, and a temperature of the glass extension (which is outside of the heater) of about 80°C. At such a low temperature, metal Rb only slightly reacts with glass. As for the interaction of Rb vapors with sapphire, no chemical interaction occurs up to temperatures of about 1000°C [15].

The wedge-shaped (vertically) thickness L of the ETC gap was determined by the interferometric method described in detail in [16] and was found to range from 100 to 600 nm. In the experiment, we used the ETC area with the gap thickness $L = 400$ nm ($\approx\lambda/2$).

2.2. Experimental Setup and Results

The scheme of the experimental setup is shown in Fig. 1a. A beam (2 mm in diameter) of a single-frequency diode laser with the wavelength $\lambda = 794$ nm (the spectral width of the radiation is about 20 MHz) was incident on the ETC window at a nearly normal angle. The ETC was placed in the center of three pairs of Helmholtz coils, which allowed us to create a uniform arbitrarily directed magnetic field of a strength B. The frequency of the laser radiation was linearly scanned in the region around the D_1 line of Rb. A Glan prism

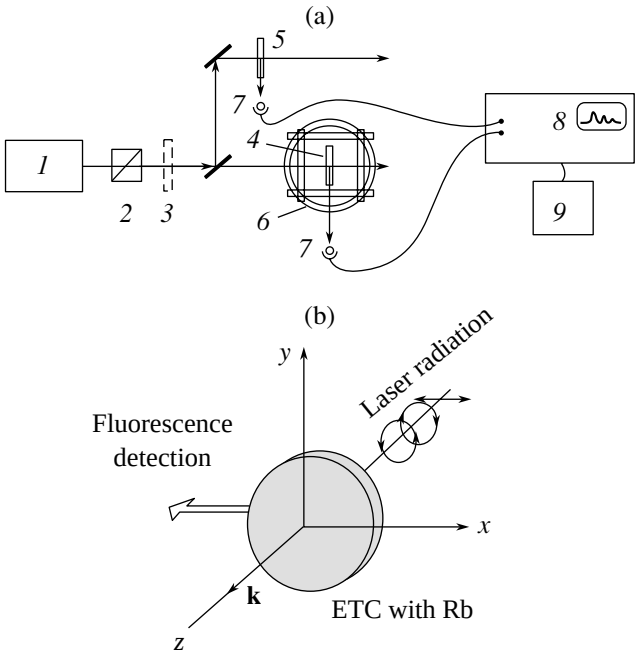

Fig. 1. (a) Schematic diagram of the optical experimental setup: (*1*) laser diode; (*2*) Glan prism; (*3*) quarter-wave plate with antireflective coating; (*4, 5*) extremely thin cells; (*6*) Helmholtz coils; (*7*) photodetectors; (*8*) Tektronix TDS 3032B oscilloscope; (*9*) computer. (b) Geometry of the magnetic measurements.

ensured a high degree of linear polarization of the pump radiation; a $\lambda/4$ plate with an antireflective coating for 780 nm was additionally used to form the circularly polarized pump radiation. A fraction (50%) of the pump radiation was sent to a second ETC with Rb (in some cases, the second ETC was replaced by an ordinary cell 1 cm long filled with rubidium), whose fluorescence spectrum was used as a frequency reference at $B = 0$. The magnetic investigations were done in the configuration presented in Fig. 1b.

The temperature of the upper edge of the Rb column was, as a rule, 120°C, which corresponds to the vapor density $N \sim 2 \times 10^{13}$ cm^{-3}. To prevent the condensation of Rb vapors on the ETC walls, the temperature of the windows was kept at a level of 140°C. The intensity of the pump radiation was about 50 mW/cm^2.

Figure 2 shows the resonance fluorescence spectra of the D_1 line of Rb at $B = 0$ for a cell 1 cm long (the upper curve) and for a ETC (the lower curve), recorded with a Tektronix TDS 3032B two-beam digital oscilloscope at room temperature. As is seen, owing to the use of the ETC, all the hyperfine transitions of ^{87}Rb and ^{85}Rb isotopes are spectrally resolved.

In the case of circular polarization of the pump radiation, σ^+ (left-handed circle) or σ^- (right-handed circle) (Fig. 1b), the magnetic field **B** was applied along the direction Z of the laser beam propagation (**B** $\parallel$ **k**). In the case of linearly polarized (π) radiation, the magnetic

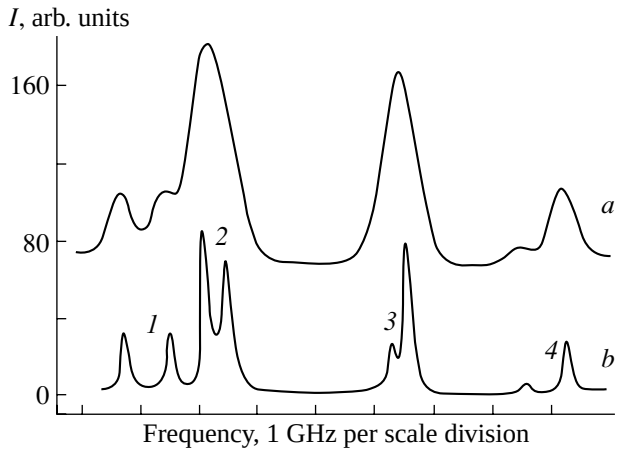

Fig. 2. Spectra of the resonance fluorescence at the Rb D_1 line at $B = 0$ for (*a*) a cell 1 cm long and (*b*) a ETC. The eight resolved peaks correspond to the transitions (*1*) ^{87}Rb, $F_g = 2 \longrightarrow F_e = 1, 2$; (*2*) ^{85}Rb, $F_g = 3 \longrightarrow F_e = 2, 3$; (*3*) ^{85}Rb, $F_g = 2 \longrightarrow F_e = 2, 3$; (*4*) ^{87}Rb, $F_g = 1 \longrightarrow F_e = 1, 2$.

field **B** was directed along the *X* axis, i.e., along the direction of polarization of the laser radiation (**B** ∥ **E**). The fluorescence of Rb vapors was recorded in the direction perpendicular to the direction of the laser beam propagation.

The diagrams of Zeeman sublevels of the transitions $F_g = 1 \longrightarrow F_e = 1, 2$ and $F_g = 2 \longrightarrow F_e = 1, 2$ of the Rb D_1 line are shown on the right-hand side of Figs. 3 and 4, respectively. The values of the level shifts are given for qualitative estimations, since, according to the calculations of the frequency positions of levels by the Breit–Rabi formula [17], the condition of the linear Zeeman effect is fulfilled well for magnetic fields up to ~50 G.

Figures 3a and 3b show the fluorescence spectra due to the $F_g = 1 \longrightarrow F_e = 1, 2$ transitions in a magnetic field with $B = 225$ G in the case of the pump radiation with σ^+ and σ^- polarization, respectively. All the fluorescence peaks in these figures can be readily identified; in particular, the five peaks in Fig. 3a correspond to the following transitions (in order of increasing frequency): $F_g = 1, m_F = -1, 0 \longrightarrow F_e = 1, m_F = 0, +1$ and $F_g = 1, m_F = -1, 0, +1 \longrightarrow F_e = 2, m_F = 0, +1, +2$. Columns in the spectra denote the calculated values of the fluorescence amplitudes and transition frequencies (see below). The fluorescence spectrum for the case of a magnetic field with $B = 225$ G and linear (π) polarization of the pump radiation is shown in Fig. 3c. In this case, all the possible transitions between the Zeeman sublevels are also spectrally resolved. Note that the transition between the magnetic sublevels $F_g = 1, m_F = 0$ and $F_e = 1, m_F = 0$ must be absent, since it is forbidden by the selection rules in the case of weak magnetic fields. However, at $B = 225$ G, this transition begins to manifest itself slightly (a short calculated column is seen in Fig. 3c).

Figure 4 demonstrates the fluorescence spectra for the transitions $F_g = 2 \longrightarrow F_e = 1,2$ in the case of the magnetic field with $B = 225$ G under excitation by the radiation with σ^+, σ^-, and π polarization. Here, similarly to the previous case, the transitions between the Zeeman sublevels can also be easily identified (seven peaks in each plot). From Fig. 4, one can see that all these transitions are spectrally resolved.

Note that, in the cell of ordinary length, all the transitions between Zeeman sublevels under the conditions considered are completely masked by the Doppler-broadened profile. Figure 5 (lower curves) demonstrates the Doppler-broadened spectra of the transitions $F_g = 1 \longrightarrow F_e = 1, 2$ and $F_g = 2 \longrightarrow F_e = 1, 2$ for a cell 1 cm long in a magnetic field with $B = 225$ G. The laser radiation has a linear (π) polarization; **B** ∥ **E**. The spectra of the resonance fluorescence at the ^{87}Rb D_1 line in the ETC (the upper curves in Fig. 5) are given as a frequency reference. It is noteworthy that the high-frequency wing of the lower curve in Fig. 5b arises rapidly owing to the influence of the high fluorescence peak corresponding to the $F_g = 2 \longrightarrow F_e = 3$ transition of ^{85}Rb (see Fig. 2), shifted to the low-frequency region by the magnetic field.

3. SIMULATION OF THE SPECTRUM AND DISCUSSION

In fact, the transitions between the Zeeman sublevels of the D_1 line of ^{87}Rb are separated in the fluorescence spectrum even in the case of fields with $B \sim 50$ G, but their complete resolution requires application of a field of about 200 G (the use of a diode laser with a spectral width of 1 MHz [16] would allow one to reduce this value). As follows from the calculations of the frequency positions of levels by the Breit–Rabi formula [17], even in the case of magnetic fields with $B > 100$ G, the frequency positions (shifts) of some peaks begin to deviate from the positions calculated in the linear Zeeman regime, which is observed in the experiment. In particular, a shift of 40 ± 5 MHz toward the high-frequency region is observed in Fig 3c for the transition $F_g = 1, m_F = 0 \longrightarrow F_e = 2, m_F = 0$, while the deviation in the linear regime should be equal to zero.

As an external magnetic field is switched on and continuously increased, it begins to break the coupling between the electron and nuclear angular momenta in the Rb atom (hyperfine interaction). Simultaneously, the wave functions of magnetic sublevels having the same value of the magnetic quantum number *m* but initially belonging to different hyperfine levels *F* are mixing. Hence, the quantum number *F* ceases to be a good quantum number, while the magnetic quantum number *m* retains its value.

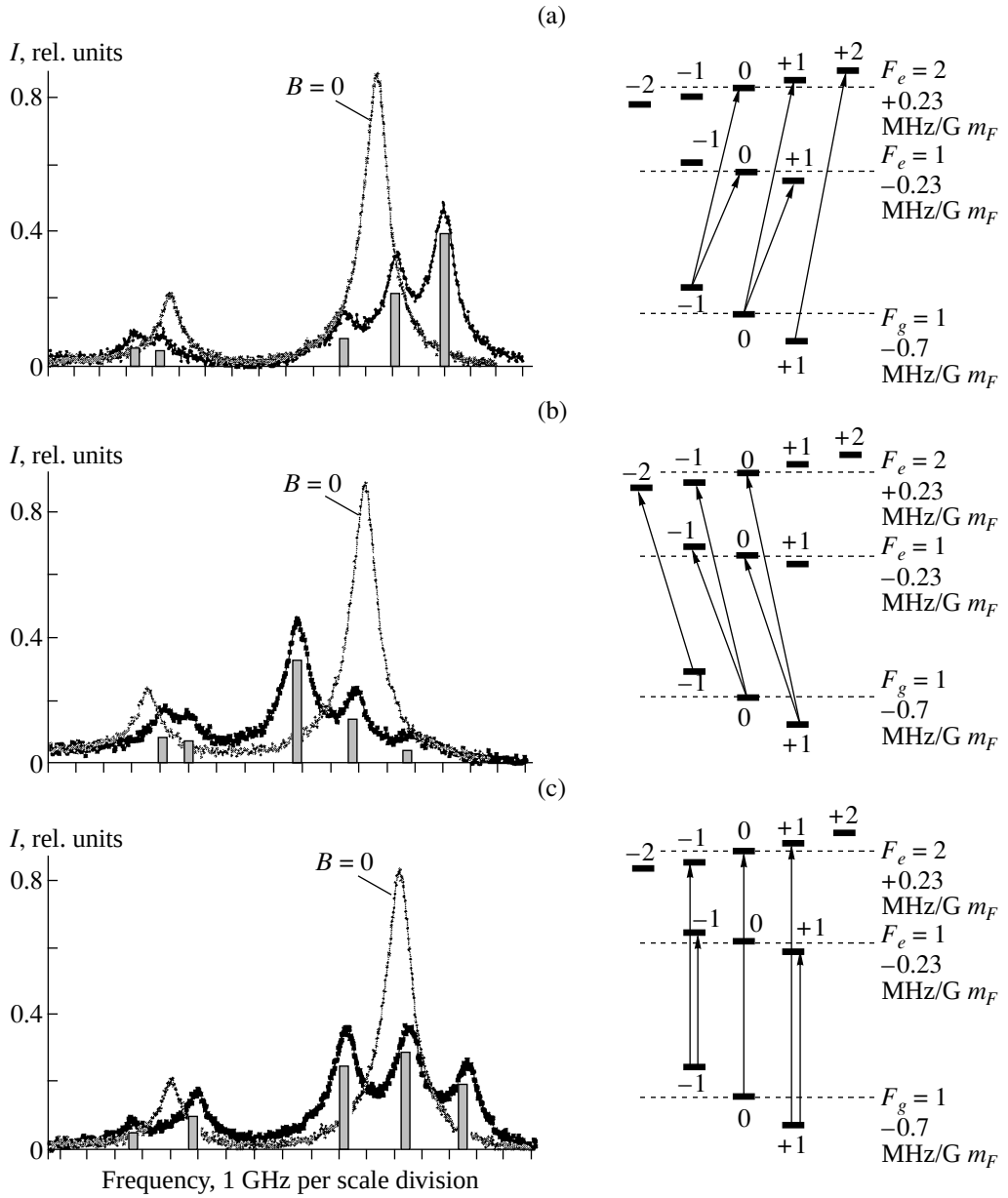

Fig. 3. Left: fluorescence spectra of the ^{87}Rb D_1 line (transitions $F_g = 1 \longrightarrow F_e = 1, 2$) for the ETC in a magnetic field of 225 G; right: diagrams of the corresponding Zeeman transitions with the values of the level shifts. The pump radiation polarization is (a) σ^+, (b) σ^-, and (c) π.

The wave functions of the magnetic sublevels of an atom in an external magnetic field can be written as

$$|\chi_e, m_e\rangle = \sum_{F_e = |J_e - I|}^{F_e = J_e + I} C^{(e)}_{\chi_e, F_e} |F_e, m_e\rangle,$$

$$|\chi_g, m_g\rangle = \sum_{F_g = |J_g - I|}^{F_g = J_g + I} C^{(g)}_{\chi_g, F_g} |F_g, m_g\rangle,$$

where the subscripts e and g correspond to the excited and ground states, χ_e and χ_g are the superposition quantum states, and C are the mixing coefficients.

As a result, the additional energy gained by the atom at a definite magnetic sublevel ceases to depend linearly on the strength of the external magnetic field. A deviation from the linear Zeeman effect takes place. In turn, the mixing of the wave functions leads to a change in the probabilities of the light absorption and emission at the transitions $F_g, m_g \longleftrightarrow F_e, m_e$, which actually are now the transitions between the χ_g, m_g and χ_e, m_e states.

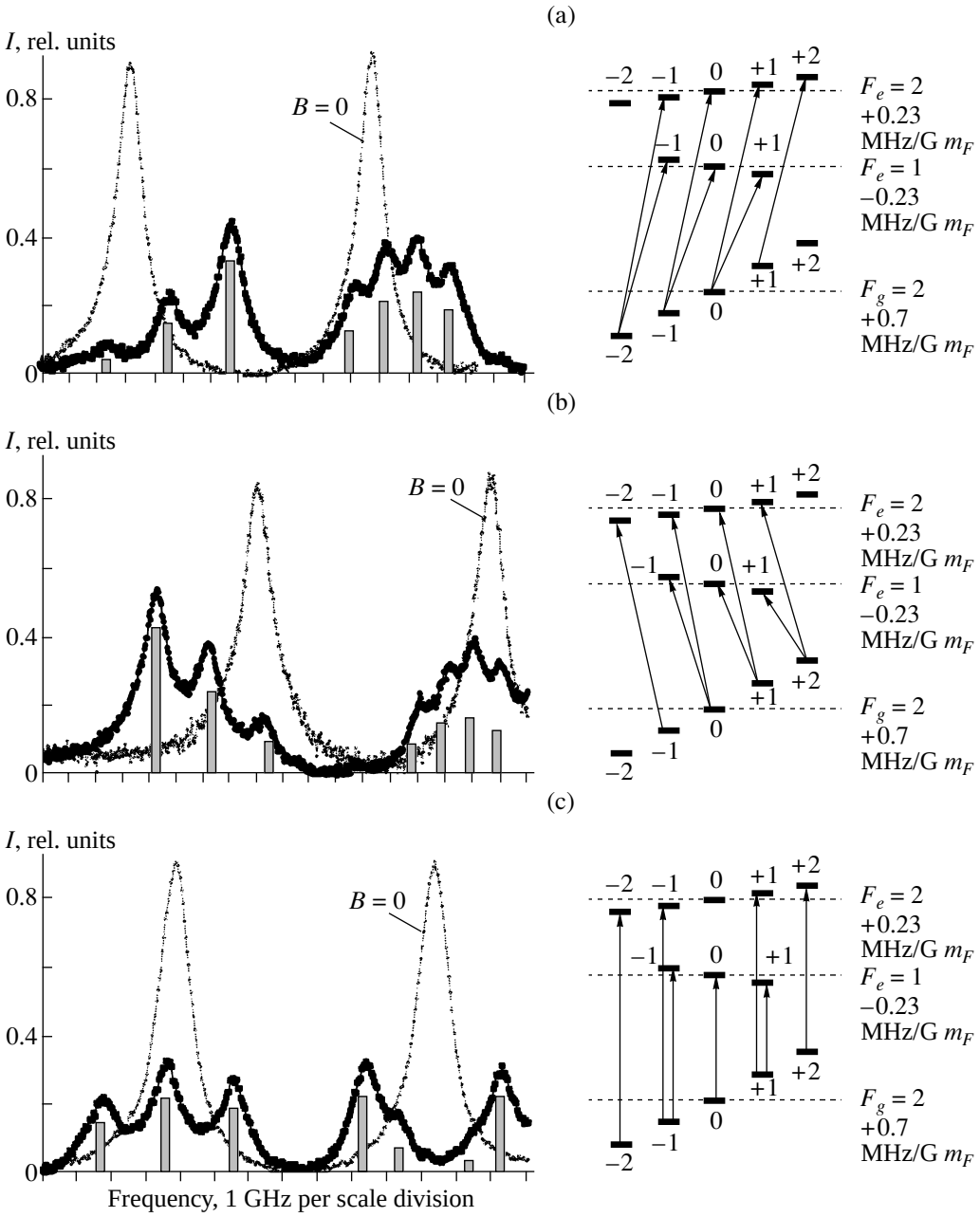

Fig. 4. Left: Fluorescence spectra of the ^{87}Rb D_1 line (transitions $F_g = 2 \longrightarrow F_e = 1, 2$) for the ETC in a magnetic field of 225 G; right: diagrams of the corresponding Zeeman transitions with the values of the level shifts. The pump radiation polarization is (a) σ^+, (b) σ^-, and (c) π.

To calculate these probabilities, one should take into account that the initial and final states of the transition are the superpositions of the hyperfine levels with different quantum numbers *F*.

In the case when the atomic state splits into only two hyperfine levels, as occurs in the case of the $S_{1/2}$ and $P_{1/2}$ levels in the Rb atom, the additional energy of magnetic sublevels, which depends nonlinearly on the external field, and the mixing of the wave functions can be calculated analytically by the Breit–Rabi formula (see, for example, [17]). In the case when the atom has more than two hyperfine levels for each electronic state, the energy of the magnetic sublevels and the mixing of the wave states should be calculated numerically on the basis of the diagonalization of the corresponding Hamiltonian matrix. For example, such a calculation for the D_2 line of Rb is described in [18].

Knowing the energies gained by different atomic states in an external magnetic field, one can calculate the spectral positions of the absorption and emission

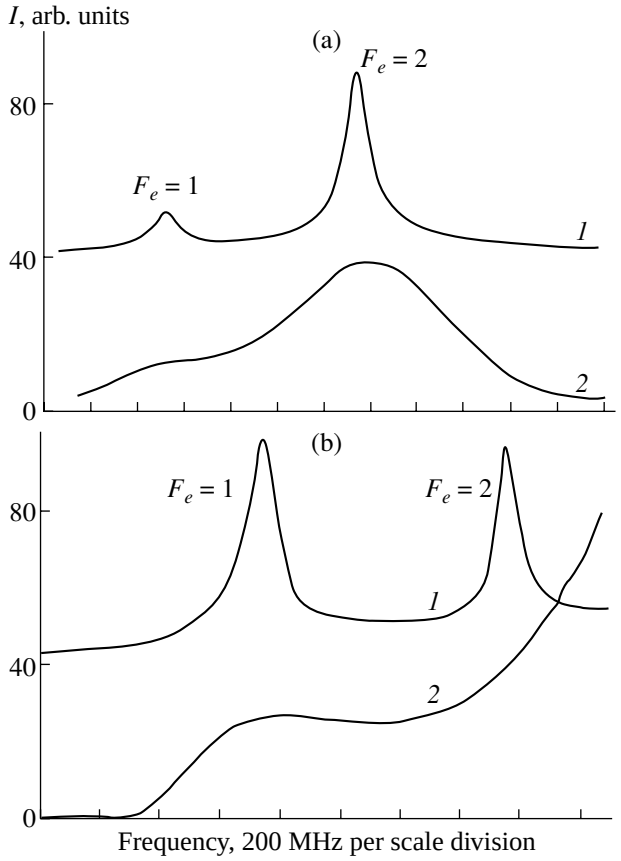

Fig. 5. (*1*) Fluorescence spectra of the D_1 line in the ETC in the absence of a magnetic field and (*2*) Doppler-broadened fluorescence spectra of a cell 1 cm long in a magnetic field of 225 G for the transitions (a) $F_g = 1 \longrightarrow F_e = 1, 2$ and (b) $F_g = 2 \longrightarrow F_e = 1, 2$.

lines for the atom in this field. In turn, knowledge of the coefficients of mixing of the wave functions enables one to calculate the probabilities of the transitions between different atomic states under excitation by light of a certain polarization, as well as the intensities of various emission lines observed in a definite direction with respect to the polarization of the pump radiation and the external magnetic field.

The calculated intensities of the spectral components of the fluorescence of the D_1 line of ^{87}Rb excited by the light of different polarizations under the conditions of our experiment are shown in Figs. 3 and 4 as vertical columns whose positions correspond to the frequencies of the pumping laser radiation, while their heights signify the total intensities of the fluorescence excited by this radiation (without spectral and frequency resolution) in the direction of the radiation detector.

Thus, the use of a ETC allows one to determine the positions of magnetic sublevels in an external magnetic field and to measure the relative probabilities of the Zeeman transitions (which may be modified in a strong magnetic field).

From Figs. 4a and 4b, it follows that the frequency spacing between the transitions $F_g = 2$, $m_F = -2 \longrightarrow F_e = 1$, $m_F = -1$ and $F_g = 2$, $m_F = +2 \longrightarrow F_e = 1$, $m_F = +1$ in a magnetic field is the largest among all the transitions and is equal to approximately 3.1 MHz/G (the calculated value in the approximation of the linear Zeeman effect is about 3.2 MHz/G). In addition, the well-defined peaks of these transitions are convenient for the creation on their basis of a simple magnetometer for the measurement of magnetic fields ranging from 50 to 500 G. In this case, despite the relatively low expected sensitivity (magnetometers with record parameters are described in [17, 19, 20]), one can achieve a submicron local spatial resolution.

CONCLUSIONS

Using the extremely thin cell with Rb vapors developed, we experimentally realized spectral resolution of individual transitions between Zeeman sublevels of the hyperfine structure of the D_1 line of ^{87}Rb (the transitions $F_g = 1, 2 \longrightarrow F_e = 1, 2$) in the spectrum of the resonance fluorescence in an external magnetic field with $B \sim 200$ G. The experimental data agree well with the theoretical calculations.

The use of a ETC in a relatively weak magnetic field allows one to obtain (and identify) nondegenerate atomic transitions between Zeeman sublevels in the fluorescence spectrum of the D_1 line of Rb. The formation of the Λ and V atomic systems consisting of nondegenerate levels, which can easily be shifted, makes the proposed ETC method convenient, for instance, for investigation of coherent population trapping [21].

On the basis of a ETC with Rb, one can design a magnetometer for the measurement of magnetic field strengths ranging from 50 to 500 G with submicron local spatial resolution.

Estimates show that the use of ETCs will also allow realization of nondegenerate atomic transitions between Zeeman sublevels in the spectra of fluorescence of the D_1 line of cesium, potassium, and other atoms. Such evident manifestation of the Zeeman levels in the case of ETCs can serve as a clear demonstration of the Zeeman effect on the hyperfine structure of alkali metal atoms.

ACKNOWLEDGMENTS

The authors are grateful to A.S. Sarkisyan for making a great contribution to the ETC preparation. This study was partially supported by the Republic of Armenia (grant nos. 1351 and 1323) and by ANSEF (grant no. PS18-01).

REFERENCES

1. S. Briaudeau, D. Bloch, and M. Ducloy, Europhys. Lett. **35**, 337 (1996).
2. S. Briaudeau, S. Saltiel, G. Nienhuis, *et al.*, Phys. Rev. A **57**, R3169 (1998).
3. S. Briaudeau, D. Bloch, and M. Ducloy, Phys. Rev. A **59**, 3723 (1999).
4. S. Briaudeau, S. Saltiel, J. R. R. Leite, *et al.*, J. Phys. IV **10**, 8 (2000).
5. A. Izmailov, Opt. Spektrosk. **74**, 41 (1993) [Opt. Spectrosc. **74**, 25 (1993)].
6. T. A. Vartanyan and D. L. Lin, Phys. Rev. A **38**, 5197 (1995).
7. B. Zambon and G. Nienhuis, Opt. Commun. **43**, 308 (1997).
8. R. H. Romer and R. H. Dicke, Phys. Rev. **99**, 532 (1955).
9. D. Sarkisyan, D. Bloch, A. Papoyan, and M. Ducloy, Opt. Commun. **200**, 201 (2001).
10. P. Tremblay, A. Nichaud, M. Levesque, *et al.*, Phys. Rev. A **42**, 2766 (1990).
11. N. Papageorgiou, A. Weis, V. A. Sautenkov, *et al.*, Appl. Phys. B **59**, 123 (1994).
12. D. G. Sarkisyan and A. V. Melkonyan, Prib. Tekh. Éksp., No. 2, 202 (1989).
13. D. G. Sarkisyan, Kvantovaya Élektron. (Moscow) **15**, 2358 (1988).
14. D. Sarkisyan, U. Hinze, L. Meyer, and B. Wellegehausen, Appl. Phys. B **70**, 351 (2000).
15. D. Sarkisyan, A. Sarkisyan, and A. Yalanusyan, Appl. Phys. B **66**, 241 (1998).
16. D. Sarkisyan, A. Papoyan, T. Varzhapetyan, *et al.*, Izv. Nats. Akad. Nauk Arm., Fiz. **37**, 342 (2002).
17. E. B. Aleksandrov, G. I. Khvostenko, and M. P. Chaĭka, *Interference of Atomic States* (Nauka, Moscow, 1991).
18. J. Alnis and M. Auzinsh, Phys. Rev. A **63**, 023407 (2001).
19. E. B. Aleksandrov, M. V. Balabas, and V. A. Bonch-Bruevich, Pis'ma Zh. Tekh. Fiz. **13**, 749 (1987) [Sov. Tech. Phys. Lett. **13**, 312 (1987)].
20. D. Budker, W. Gawlik, D. Kimball, *et al.*, Rev. Mod. Phys. **74**, 1153 (2002).
21. D. M. Petrosyan and Yu. P. Malakyan, Phys. Rev. A **61**, 053820 (2000).

Translated by M. Basieva